Asynchronous Reception of 2 RFID Tags

Konstantinos Skyvalakis and Aggelos Bletsas, *Senior Member, IEEE*

***Abstract*—Commercial radio frequency identification (RFID) readers have to resolve collisions between tags, without sacrificing throughput. This work proposes a Viterbi *joint sequence detector* as well as a 2-symbol joint tag information detector that can resolve a collision between two tags in the physical layer. In sharp contrast to prior art, the proposed closed-form signal model takes into account the asynchrony level between the two collided tag responses, which is not uncommon with commercial, low-cost RFID tags that follow industry's Gen2 protocol. The asynchrony is considered as the time offset τ between the beginnings of the two tags' responses and is modeled through a derived *shaping* matrix that depends on the delayed tag information. Performance evaluation of the proposed detectors with simulated data under Ricean fading, as well as experimental data with software-defined radio, reveals improved performance compared to prior art, under various operating regimes. It is also shown that for different values of the parameter τ, BER does not present a monotonic behaviour. As a collateral dividend, it is found that clustering techniques on the *filtered* received signal should explicitly take into account the time offset τ, since the latter modifies the number of observed clusters.**

***Index Terms*—Asynchronous Detection, Symbol Synchronization, Viterbi, FM0, RFID, Gen2.**

I. Introduction

As the number of deployed batteryless radio frequency identification (RFID) / internet-of-things (IoT) tags is constantly increasing, academic and industrial research has been examining ways to accelerate the inventorying process and improve efficiency and throughput.

Tag singulation is facilitated in the commercial Gen2 standard [1], using framed slotted Aloha (FSA), where tags *compete* using pseudo-random 16-bit sequences (plus common preamble information), named as RN16; the tag that *wins* the slot, transmits its 96-bit ID information (EPC) in a subsequent time step, while the rest of the competing tags back off; when two or more tags respond simultaneously, the tags' RN16 packets collide mid-air, which may result to incorrect detection and erroneous acknowledgment of tag's RN16 from the reader; in that case, the tag does not transmit its EPC and a whole frame is wasted, resulting to inventorying rate drop. Thus, collision among two or more tags occurs during the RN16 transmission stage and thus, anti-collision techniques focus on that part of information. Fig. 1-left depicts such collision case, with inphase (I) and quadrature (Q) signals collected experimentally; the reader transmits a query, a number of tags respond at the same slot, the RN16 is not decoded properly at the reader and no tag receives a valid acknowledgement with its transmitted RN16 information; thus, no tag transmits its ID information (EPC) subsequently.

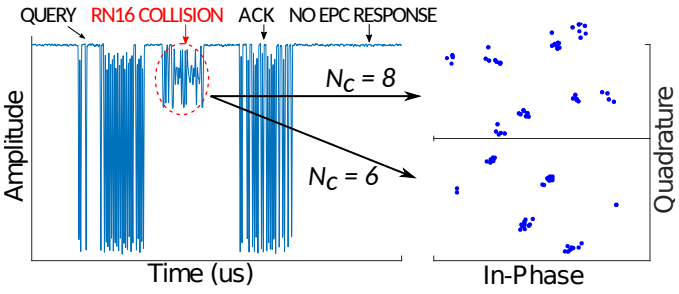

Fig. 1: RN16 collision of 2 tags resulting in 6 or 8 clusters. Plot was offered after experimentation with 2 commercial tags and the software stack from work in [2].

Assuming FSA with N tags competing for L slots, the probability of exactly q tags (out of N) choosing the same slot is simply given through the binomial: $\Pr(q) = \binom{N}{q}(1/L)^q(1-1/L)^{N-q}$. Therefore, the probability of collision is given by $\Pr(q=2) + \Pr(q=3) + \ldots = \sum_{q=2}^{\infty} \Pr(q)$. For practical setups, where the reader selects a relatively large number of slots, the collision probability is dominated by $\Pr(q=2)$, i.e., the probability that exactly two tags' RN16 information is transmitted at the same slot. Specifically, probability of more than two tags (i.e., *at least* three tags) collide at the same slot $\sum_{q=3}^{\infty} \Pr(q) = 1 - \Pr(q=0) - \Pr(q=1) - \Pr(q=2)$ is given at Fig. 2, for various number of tags N and slots L; it can be safely said that collision probability from more than 2 tags drops below 1% for reasonable numbers of N, L. Furthermore, even if the reader could correctly detect all tags' RN16 information, it would acknowledge only one of them, according to Gen2; thus, better joint detection of all collided tags would not necessarily offer increased throughput. Therefore, the case of 2 tag's collision in Gen2 is important, *both* from a theoretical *and* practical standpoint.

Following the high demand for successful inventorying of backscatter-based tags and sensors, as quickly and efficiently as possible, prior art [3] has analyzed the constellation of tag signals colliding in a single slot, leveraging clustering techniques for up to four colliding tag signals. However, this work was initially developed for low frequency (LF) tags and could be extended to Gen2 RFID tags. The authors in [4], [5] proposed a zero-forcing (ZF) receiver that treats one of the two RN16 responses as interference, and projects the signal constellation into the subspace that completely cancels that interference. Work in [6], [7] proposed ZF and minimum mean squared error (MMSE) receivers, exploiting multiple receiving antennas and additional reference bits, not currently present in Gen2, that could assist channel estimation.

This research has been co-financed by the European Union and Greek national funds through the Operational Program Competitiveness, Entrepreneurship and Innovation, under the call RESEARCH - CREATE - INNOVATE (project code: T1EDK-03032). Authors are with School of ECE, Technical Univ. of Crete, Chania, Greece 73100. Email: {kskyvalakis@isc.tuc.gr, aggelos@telecom.tuc.gr}

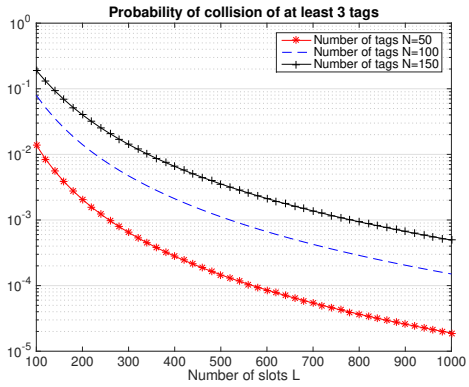

Fig. 2: Probability of collision from more than 2 tags (i.e., 3 or more) in slotted Aloha of L slots, among N tags. Notice that such probability can drop below 1% for reasonable numbers of N and L.

Work in [8] proposed a detection technique for collision of multiple FM0 or Miller RFID line-encoded signals, based on Viterbi, designed for *single-tag* detection using Viterbi and successive interference cancellation (SIC). Initially, a single tag reply is assumed and an estimate of the symbol period and the delay offset is obtained by employing a correlation-based method. Then, single-tag maximum likelihood sequence detector (i.e., Viterbi) is applied to decode the single tag's information, in sharp contrast to this work, which designs a joint Viterbi detector for both tags. Finally, an estimate of the tag's contribution is generated and subtracted from the residual and the same process is repeated until termination. As in every SIC-based technique, the above method is sensitive to the power ratio among the tags.

Work in [9] proposed multiple access based on rateless codes, which is closer to code division multiple access (CDMA). Frequency domain multiple access (FDMA), based on different subcarrier per tag, i.e., different switching rate of each tag among two termination loads, has been proposed and experimentally demonstrated in [10] using minimum shift keying (MSK), also showcasing that efficient spectrum shaping can be achieved with only two loads per tag and a common carrier frequency at the reader. Both aforementioned techniques depart from the time division multiple access (TDMA) flavour of FSA in Gen2.

Work in [11], [12] proposed a new protocol (different than Gen2), resolving tag collisions by separating the signals' edges in the time domain, while also leveraging the I/Q samples to further clarify any ambiguities that might occur due to the asynchronous character of the system. Work in [13] follows a similar approach to [12] but focuses on Gen2. In [14], the authors claim that the signals' combined states follow highly stable probabilities; transitions between the clusters in the I/Q plane are tracked, decoding the individual packets involved in the collision, without the need to track signals' edges in the time-domain. Work in [14] is extended in [15], which proposes exploitation of the spatiotemporal distribution of the collided signals. Finally, work in [16] proposes a multi-antenna blind beamforming technique, which however does not take into account the impact of asynchrony on the number of observed I/Q clusters.

In sharp contrast to prior art, this work offers a closed-form system model, which explicitly takes the time offset between the responses of the two tags into consideration, rather than neglecting it. Even though the tags always respond to the reader commands, it has been experimentally observed that their response to the reader messages is not instant but time-variable and thus, different, probably due to their ultra-low cost hardware. The offered detectors are built upon the proposed closed-form signal model and take into account the time offset between the two tags, modeled through the use of a shaping matrix. Given that all reception techniques involve some type of filtering to improve signal-to-noise (SNR) ratio (e.g., matched filtering), plotting the filtered samples of the received signal offers information about the existence of such asynchrony.

More specifically, a collision in the physical layer between two Gen2 RFID tag RN16 responses, can either result in 4, 6 or 8 clusters in the I/Q plane, *after* matched filtering of the received signal and then, plotting the real and imaginary part, experimentally shown in Fig. 1-right and explained through formal proofs in this work. Fig. 1 was offered after experimentation with commodity software-defined radio (SDR) and Gen2 RFID tags. After matched filtering, 4 clusters can be observed when the 2 tags are perfectly time-synchronized (i.e., time offset is zero) or when one of them is lagging by a half-bit period, $T/2$, while the 6 and 8 clusters cases, also shown in Fig. 1, occur for the remaining time offset values between 0 and T. Thus, collision resolution based on clustering methods should take into account such reality. Extensive experimental tests at the lab, interrogating 10000 times 2 commercial Gen2 RFID tags corroborated the above: 57% of the time the 2 tags were out of sync, while an astounding 98% of those asynchronous collisions generated more than 4 clusters on the I/Q plane, after matched filtering.

The contributions of this work are summarized below:

- Detection techniques are offered that explicitly take into account tag asynchrony, i.e., the time offset τ between two tags, which is not uncommon with commercial, low-cost RFID tags;
- It is shown that the proposed asynchronous detection techniques with estimated CSI and τ can offer BER in certain regimes that renders the detection of the 16 bits from one of the two tags RN16 message, error free. Moreover, the value of τ in the detectors' performance is important and presents an oscillating behaviour;
- It is shown that there exists a small performance gap of the proposed $2T$ detectors, i.e., detectors that utilize signal duration of 2 symbols, compared to Viterbi for joint tag detection in the asynchronous case; such performance gap is relatively small and due to the extra induced memory from the delayed second tag; it was also found that the proposed $2T$ detectors performed as well as Viterbi in the synchronous case;
- Practical algorithm for time offset estimation is offered. It is shown that symbol detection, packet synchronization

and channel estimation must be revisited in asynchronous multiple access systems, as in this work.
- As a collateral dividend, it is shown that clustering techniques on the *filtered* received signal should explicitly take into account the time offset τ, that modifies the number of observed clusters.
- Performance evaluation is conducted with simulation as well as experimental data, using commodity Gen2 RFID tags and implementation of the proposed scheme in C++ and software-defined radio.

Section II offers the system model; Section III presents transformation of the problem; Section IV offers the detection techniques, while Section V offers necessary housekeeping, i.e., DC, channel and delay estimation techniques utilized in this work; Section VI presents the numerical results; finally, work is concluded in Section VII.

Notation: Symbols $\mathbb{N}$, $\mathbb{R}$, and $\mathbb{C}$ denote the set of natural, real, and complex numbers, respectively. $\mathbf{0}_N$ and $\boldsymbol{I}_N$, denote the all-zeros vector and identity matrix of size N, respectively. The phase of complex number z is denoted as $\angle z$, while $\Re\{z\}$ and $\Im\{z\}$ denote the real and imaginary part of z, respectively. The distribution of a proper complex Gaussian $N \times 1$ vector $\boldsymbol{x}$ with mean $\boldsymbol{\mu}$ and covariance matrix $\boldsymbol{\Sigma}$ is denoted by $\mathcal{CN}(\boldsymbol{\mu}, \boldsymbol{\Sigma}) \triangleq \frac{1}{\pi^N \det(\Sigma)} \mathrm{e}^{-(\boldsymbol{x}-\boldsymbol{\mu})^H \boldsymbol{\Sigma}^{-1}(\boldsymbol{x}-\boldsymbol{\mu})}$; the special case of a circularly symmetric complex Gaussian $N \times 1$ vector corresponds by definition to $\mathcal{CN}(\mathbf{0}_N, \boldsymbol{\Sigma})$; $\mathcal{U}[a, b)$ denotes the uniform distribution in $[a, b)$. Expectation of function $\mathrm{g}(\cdot)$ of continuous random variable x with probability density function (PDF) $\mathrm{f}_x(\cdot)$ is denoted as $\mathbb{E}[\mathrm{g}(x)] \triangleq \int_x \mathrm{g}(x)\mathrm{f}_x(x)\mathrm{d}x$. $\mathbb{1}(\mathcal{C})$ denotes the indicator function, which equals 1 when condition $\mathcal{C}$ is true and 0 otherwise.

II. System Model

A. Channel Model

The following *large-scale* channel path-loss model is adopted [17]:

$$\mathsf{L}_{\mathrm{k}} = \left(\frac{\lambda}{4\pi d_0}\right)^2 \left(\frac{d_0}{d_{\mathrm{k}}}\right)^{v_{\mathrm{k}}}, \tag{1}$$

where $\mathrm{k} \in \{\mathrm{CR}, \mathrm{CT}_m, \mathrm{T}_m\mathrm{R}\}$ denotes the carrier emitter-to-reader, carrier emitter-to-tag and tag-to-reader link, respectively, λ is the carrier wavelength, d_0 is a reference distance and v_{k} is the path-loss exponent for link k. Moreover, a monostatic setup is assumed, corresponding to $\mathsf{L}_{\mathrm{CT}_m} = \mathsf{L}_{\mathrm{T}_m\mathrm{R}}$.

Due to strong line-of-sight (LoS) signals present in this problem, *small-scale* Rice flat fading channel model [17] is adopted; end-2-end complex channel gain for tag $m \in \{a, b\}$ is denoted as follows:

$$h_m = h_{\mathrm{CT}_m}\, h_{\mathrm{T}_m\mathrm{R}} = |h_{\mathrm{CT}_m}\, h_{\mathrm{T}_m\mathrm{R}}|\, e^{-j\phi_m} \in \mathbb{C}, \tag{2}$$

where h_{CT_m} and $h_{\mathrm{T}_m\mathrm{R}}$ denotes the baseband complex channel coefficients for the carrier emitter-tag and tag-reader link, respectively; furthermore, $h_m \in \mathbb{C}$, $|h_{\mathrm{CT}_m}\, h_{\mathrm{T}_m\mathrm{R}}| \in \mathbb{R}_+$ and $\phi_m \in [0, 2\pi)$. Due to the monostatic architecture assumed, reciprocity implies $h_{\mathrm{T}_m\mathrm{R}} = h_{\mathrm{CT}_m}$ and due to the Rice channel fading assumption,

$$h_{\mathrm{T}_m\mathrm{R}} \sim \mathcal{CN}\left(\sqrt{\frac{\kappa_m}{\kappa_m+1}}\,\sigma_{h_{\mathrm{T}_m\mathrm{R}}}, \frac{\sigma^2_{h_{\mathrm{T}_m\mathrm{R}}}}{\kappa_m+1}\right), \tag{3}$$

where $\mathbb{E}[|h_{\mathrm{T}_m\mathrm{R}}|^2] = \sigma^2_{h_{\mathrm{T}_m\mathrm{R}}}$ is the average power of the scattering components and $\kappa_m = k_{\mathrm{T}_m\mathrm{R}} = k_{\mathrm{CT}_m}$ is the power ratio between the deterministic LoS component and the scattering components. For link budget normalization purposes, $\mathbb{E}[|h_m|^2] = \mathbb{E}[|h_{\mathrm{T}_m\mathrm{R}}|^4] = 1$ will be also assumed.

B. Signal Model

The reader transmits a sinusoidal carrier wave, whose complex baseband equivalent representation is given by:

$$c(t) = \sqrt{2P_c}\, e^{-j(2\pi\Delta F\, t + \Delta\phi)}, \quad \Delta\phi \sim \mathcal{U}[0, 2\pi), \tag{4}$$

where ΔF, $\Delta\phi$ denotes the carrier frequency offset (CFO) and the phase offset, respectively, compared to the receiver and P_c the power of the carrier wave.

Two tags will be assumed: tag a and tag b. The baseband complex equivalent of the scattered waveform from tag $m \in \{a, b\}$ is given by, [18]:

$$u_m(t) = \sqrt{\eta\, \mathsf{L}_{\mathrm{CT}_m}}\, [(A_s - \Gamma_0) + (\Gamma_0 - \Gamma_1) x_m(t)]\, h_{\mathrm{CT}_m} c(t), \tag{5}$$

$$h_{\mathrm{CT}_m} = |h_{\mathrm{CT}_m}|\, e^{-j\phi_{\mathrm{CT}_m}}, \quad \phi_{\mathrm{CT}_m} \in [0, 2\pi), \tag{6}$$

where $x_m(t) \in \{0, 1\}$, η models tag power scattering efficiency and Γ_0, Γ_1 stands for the reflection coefficients for bit "0" and bit "1", respectively; parameter A_s stands for the load-independent *structural mode* that solely depends on tag's antenna [19].

For the duration T of a single bit, the received demodulated complex baseband signal at the SDR reader is given by the superposition of the carrier emitter (CE) sinusoid and the tags' backscattered signals propagated through wireless channels h_{CR} and $h_{\mathrm{T}_m\mathrm{R}}$, respectively:

$$\begin{aligned}
y(t) &= \sqrt{\mathsf{L}_{\mathrm{CR}}}\, |h_{\mathrm{CR}}| e^{-j\phi_{\mathrm{CR}}} c(t) + \sqrt{\mathsf{L}_{\mathrm{T}_a\mathrm{R}}}\, |h_{\mathrm{T}_a\mathrm{R}}| e^{-j\phi_{\mathrm{T}_a\mathrm{R}}}\, u_a(t) \\
&+ \sqrt{\mathsf{L}_{\mathrm{T}_b\mathrm{R}}}\, |h_{\mathrm{T}_b\mathrm{R}}|\, e^{-j\phi_{\mathrm{T}_b\mathrm{R}}}\, u_b(t) + n(t) \\
&= \Big[\sqrt{2P_c}\, e^{-j\Delta\phi} \Big(\sqrt{\mathsf{L}_{\mathrm{CR}}}\, |h_{\mathrm{CR}}|\, e^{-j\phi_{\mathrm{CR}}} \\
&+ \sqrt{\eta\, \mathsf{L}_{\mathrm{CT}_a}\, \mathsf{L}_{\mathrm{T}_a\mathrm{R}}}\, (A_s - \Gamma_0)\, |h_{\mathrm{CT}_a}\, h_{\mathrm{T}_a\mathrm{R}}|\, e^{-j(\phi_{\mathrm{CT}_a} + \phi_{\mathrm{T}_a\mathrm{R}})} \\
&+ \sqrt{\eta\, \mathsf{L}_{\mathrm{CT}_b}\, \mathsf{L}_{\mathrm{T}_b\mathrm{R}}}\, (A_s - \Gamma_0)\, |h_{\mathrm{CT}_b}\, h_{\mathrm{T}_b\mathrm{R}}|\, e^{-j(\phi_{\mathrm{CT}_b} + \phi_{\mathrm{T}_b\mathrm{R}})}\Big) \\
&+ \sqrt{2\,\eta\, P_c}\, (\Gamma_0 - \Gamma_1)\, \Big(\sqrt{\mathsf{L}_{\mathrm{CT}_a}\, \mathsf{L}_{\mathrm{T}_a\mathrm{R}}}\, |h_{\mathrm{CT}_a}\, h_{\mathrm{T}_a\mathrm{R}}|\, e^{-j\phi_a} x_a(t) \\
&+ \sqrt{\mathsf{L}_{\mathrm{CT}_b}\, \mathsf{L}_{\mathrm{T}_b\mathrm{R}}}\, |h_{\mathrm{CT}_b}\, h_{\mathrm{T}_b\mathrm{R}}| e^{-j\phi_b} x_b(t)\Big)\Big]\, e^{-j2\pi\Delta F t} + n(t).
\end{aligned} \tag{7}$$

Notice that the term inside the brackets of Eq. (7) consists of a complex, time-independent DC offset plus two tag/time-dependent terms.

Due to the fact that the receiver and the emitter share the same oscillator, $\Delta F = \Delta\phi = 0$ are assumed zero in the monostatic case. It is further assumed that the receiver/reader

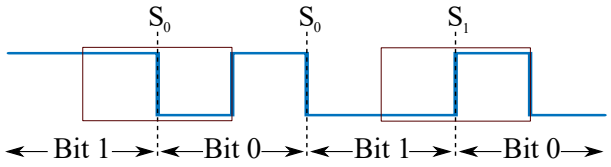

Fig. 3: FM0 line-coded waveform of a single tag.

can estimate and remove the DC offset, Eq. (7) (with the help of Eq. (2)) is simplified to the following DC-blocked received signal during bit period T:

$$\tilde{y}(t) = h_a\,\mu_a\,x_a(t) + h_b\,\mu_b\,x_b(t) + n(t), \tag{8}$$

where parameter μ_m incorporates the compound scatter radio link path-losses and tag-related parameters,

$$\mu_m = \sqrt{2\,\eta\,P_c}\,\mathsf{L}_{\mathrm{T}_m\mathrm{R}}\,(\Gamma_0 - \Gamma_1),\ m \in \{a, b\}, \tag{9}$$

and $n(t)$ stands for the additive thermal noise at the receiver, modeled by a complex, circularly symmetric, additive Gaussian noise process with the following power spectral density:

$$S_{nn}(F) = \begin{cases} \frac{N_0}{2}, & |F| \le W \\ 0, & \text{otherwise} \end{cases}, \tag{10}$$

where W stands for receiver's bandwidth.[1]

C. FM0 Line Coding

Nominal bit duration is denoted by T and sampling period by T_s; oversampling factor $L \triangleq \frac{T}{T_s}$ (not to be confused with path-loss model L_k) is assumed, without loss of generality, to be an even number.

An example of FM0 line coding is shown Fig. 3; line always changes level at bit boundaries and at the middle of bit '0'. After shifted examination of the transmitted waveform by $T/2$ before the beginning of the bit for a single user/tag FM0 and observing signal of duration T, only one of the following waveforms can be observed, $S_0(t), S_1(t)$ (instead of four), marked in Fig. 3 with rectangles:

$$S_0(t) = \begin{cases} 1, & \text{if } 0 \le t < \frac{T}{2} \\ 0, & \text{if } \frac{T}{2} \le t < T \end{cases},\ S_1(t) = \begin{cases} 0, & \text{if } 0 \le t < \frac{T}{2} \\ 1, & \text{if } \frac{T}{2} \le t < T \end{cases}. \tag{11}$$

Taking into account the memory induced by FM0, ML sequence detection rule is simplified to observing $2T$-signal duration for each bit of duration T [20], [21]; assuming $\hat{d} = 0$ ($\hat{d} = 1$) if $S_0(t)$ ($S_1(t)$) is detected,[2] the final decision for the transmitted bits b is computed as follows:

$$\hat{b}(n) = \hat{d}(n-1) \oplus \hat{d}(n), \tag{12}$$

where $\oplus$ is the xor operator, $\hat{d}(-1) = 0$ and $\hat{d}(n-1), \hat{d}(n)$ correspond to decisions for two consecutive time-shifted (by $T/2$) FM0 waveforms of duration T each. In other words, observation and processing of $2T$-signal duration suffices for optimal ML sequence detection [20], [21] and thus, for FM0 there is no need to run the Viterbi algorithm in a single-tag scenario.

[1] $N_0 = k_b T_\theta$, where k_b and T_θ are the Boltzmann constant and receiver temperature, respectively

[2] $S_0(t)$ corresponds to $\boldsymbol{e}_0 = [1\ 0]^T$ and $S_1(t)$ corresponds to $\boldsymbol{e}_1 = [0\ 1]^T$.

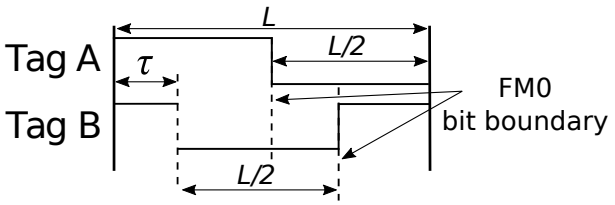

Fig. 4: Tag a backscatters $S_0(t)$ that corresponds to $\boldsymbol{x}_{a,i} = \boldsymbol{e}_0$. Tag b backscatters $S_1(t)$, delayed by τ samples, corresponding to $\boldsymbol{x}_{b,i} = \boldsymbol{e}_1$. Immediately before that, tag b backscatters $S_1(t)$, which corresponds to $\boldsymbol{x}_{b,i-1} = \boldsymbol{e}_1$.

The received signal $\tilde{y}(t)$ is sampled at each $kT_s, k \in \mathbb{N}$, offering $\tilde{y}[k] \equiv \tilde{y}(kT_s)$ and then filtered using a square pulse $\Pi[k]$ of length $L/2$ as follows:

$$y_f[n] = \sum_{k=-\infty}^{\infty} \tilde{y}[k]\Pi[n-k]. \tag{13}$$

In sharp contrast to prior art, this work considers a non-zero time offset between the two tags $\tau' \in \{0, T_s, 2T_s, \ldots, T - T_s\}$, that renders conventional detection suboptimal. Equivalently, the asynchrony can be represented by number of samples $\tau \in \{0, 1, 2, \ldots, L-1\}$, as depicted in Fig. 4.

III. Problem Transformation

Fig. 4 depicts shifted by $T/2$ observation of tag a signal, where $S_0(t)$ is backscattered, while tag b backscatters with a delay of $\tau < L/2$ samples waveform $S_1(t)$, preceded by $S_1(t)$. The following theorem puts forth asynchronous detection, simplifying the problem in a compact way:

Theorem 1. *Assuming perfect symbol synchronization w.r.t. tag a and shifted by $T/2$ observation (as in Fig. 4), the asynchronous, baseband equivalent model (after pulse matched filtering), including information $\boldsymbol{x}_{a,i}$, $\boldsymbol{x}_{b,i}$ from tag a and b, respectively, during the $i-th$ FM0 symbol, as well as tag's b previous information symbol $\boldsymbol{x}_{b,i-1}$, is given as follows:*

$$\boldsymbol{y}_i = h_a \sqrt{\frac{\mathcal{E}^a_{bit}}{\mathbb{E}[|h_a|^2]}}\,\boldsymbol{x}_{a,i} + \boldsymbol{B}_{(i-1,i)}\,h_b \sqrt{\frac{\mathcal{E}^b_{bit}}{\mathbb{E}[|h_b|^2]}}\,\boldsymbol{x}_{b,i} + \boldsymbol{n}_i, \tag{14}$$

where $\boldsymbol{n}_i \sim \mathcal{CN}(\boldsymbol{0}_2, \underbrace{N_0 W T_s}_{\sigma^2}\boldsymbol{I}_2) \equiv \mathcal{CN}(\boldsymbol{0}_2, \sigma^2\boldsymbol{I}_2)$, $\boldsymbol{x}_{a,i},\ \boldsymbol{x}_{b,i} \in \{\boldsymbol{e}_0, \boldsymbol{e}_1\}$, *with*

$$\boldsymbol{e}_0 \triangleq \begin{bmatrix} 1 \\ 0 \end{bmatrix},\ \boldsymbol{e}_1 \triangleq \begin{bmatrix} 0 \\ 1 \end{bmatrix}, \tag{15}$$

and shaping matrix $\boldsymbol{B}_{(i-1,i)} \in \mathbb{R}^{2\times 2}$, detailed in Table I, is a function of $\boldsymbol{x}_{b,i}$, $\boldsymbol{x}_{b,i-1}$ and $\tau \in \{0, 1, \ldots, L-1\}$:

$$\boldsymbol{B}_{(i-1,i)} \equiv \boldsymbol{B}\,(\tau, \boldsymbol{x}_{b,i-1}, \boldsymbol{x}_{b,i})\,.$$

Proof. The proof is given in Appendix A. ■

TABLE I: Shaping matrices $\boldsymbol{B}_{(i-1,i)}$.

$\tau < L/2$		
	$\boldsymbol{x}_{b,i} = [1\ 0]^T$	$\boldsymbol{x}_{b,i} = [0\ 1]^T$
$\boldsymbol{x}_{b,i-1} = \begin{bmatrix}1\\0\end{bmatrix}$	$\boldsymbol{B}_1 = \begin{bmatrix}1-\frac{2\tau}{L} & 0\\ \frac{2\tau}{L} & 0\end{bmatrix}$	$\boldsymbol{B}_2 = \begin{bmatrix}0 & 0\\ 0 & 1-\frac{2\tau}{L}\end{bmatrix}$
$\boldsymbol{x}_{b,i-1} = \begin{bmatrix}0\\1\end{bmatrix}$	$\boldsymbol{B}_3 = \begin{bmatrix}1 & 0\\ \frac{2\tau}{L} & 0\end{bmatrix}$	$\boldsymbol{B}_4 = \begin{bmatrix}0 & \frac{2\tau}{L}\\ 0 & 1-\frac{2\tau}{L}\end{bmatrix}$
$\tau \geq L/2$		
$\boldsymbol{x}_{b,i-1} = \begin{bmatrix}1\\0\end{bmatrix}$	$\boldsymbol{B}_1 = \begin{bmatrix}\frac{2\tau}{L}-1 & 0\\ 2-\frac{2\tau}{L} & 0\end{bmatrix}$	$\boldsymbol{B}_2 = \begin{bmatrix}0 & \frac{2\tau}{L}-1\\ 0 & 0\end{bmatrix}$
$\boldsymbol{x}_{b,i-1} = \begin{bmatrix}0\\1\end{bmatrix}$	$\boldsymbol{B}_3 = \begin{bmatrix}2-\frac{2\tau}{L} & 0\\ 1 & 0\end{bmatrix}$	$\boldsymbol{B}_4 = \begin{bmatrix}0 & 2-\frac{2\tau}{L}\\ 0 & \frac{2\tau}{L}-1\end{bmatrix}$

TABLE II: Transmitted symbol combinations.

$\boldsymbol{x}_{a,i}$	$\boldsymbol{e}_0$	$\boldsymbol{e}_1$	$\boldsymbol{e}_0$	$\boldsymbol{e}_1$	$\boldsymbol{e}_0$	$\boldsymbol{e}_1$	$\boldsymbol{e}_0$	$\boldsymbol{e}_1$
$\boldsymbol{x}_{b,i}$	$\boldsymbol{e}_0$	$\boldsymbol{e}_1$	$\boldsymbol{e}_1$	$\boldsymbol{e}_0$	$\boldsymbol{e}_0$	$\boldsymbol{e}_1$	$\boldsymbol{e}_1$	$\boldsymbol{e}_0$
$\boldsymbol{x}_{b,i-1}$	$\boldsymbol{e}_0$	$\boldsymbol{e}_0$	$\boldsymbol{e}_0$	$\boldsymbol{e}_0$	$\boldsymbol{e}_1$	$\boldsymbol{e}_1$	$\boldsymbol{e}_1$	$\boldsymbol{e}_1$
$\boldsymbol{B}_{(i-1,i)}$	$\boldsymbol{B}_1$	$\boldsymbol{B}_2$	$\boldsymbol{B}_2$	$\boldsymbol{B}_1$	$\boldsymbol{B}_3$	$\boldsymbol{B}_4$	$\boldsymbol{B}_4$	$\boldsymbol{B}_3$

As detailed in Table I, eight different values for matrix $\boldsymbol{B}_{(i-1,i)}$ are possible. The first and second row of $\boldsymbol{B}_{(i-1,i)}$ corresponds to y_0^i and y_1^i, respectively, also encompassing the part of the detection window, where signal from tag b is present. The first and second column corresponds to tag b emitting $\boldsymbol{x}_{b,i} = [1\ 0]^T$ or $\boldsymbol{x}_{b,i} = [0\ 1]^T$, respectively. By definition, a signal like $\boldsymbol{x}_{b,i} = [1\ 1]^T$ can never be observed, therefore one column will always be filled with zeros. Table II encodes the possible (output) values of matrix $\boldsymbol{B}_{(i-1,i)}$, as a function of tag b's consecutive information $\boldsymbol{x}_{b,i-1}$, $\boldsymbol{x}_{b,i}$.

A. Number of clusters

The number of clusters observed in the I/Q plane, after processing a number of samples of the received signal as in Eq. (13) or Eq. (14), varies for different values of τ. More specifically, $\tau \in \left\{0, \frac{L}{2}\right\}$ produces 4 clusters, $\tau \in \left\{\frac{L}{4}, \frac{3L}{4}\right\}$ produces 6 clusters, while the remaining values $\tau \in \{0, \ldots, L-1\} / \left\{0, \frac{L}{4}, \frac{L}{2}, \frac{3L}{4}\right\}$ produce 8 clusters, after plotting the y_f samples every $k\frac{L}{2}$, $k \in \mathbb{N}$, as in Fig. 1.[3] Even though this paper does not utilize any clustering techniques, this observation highlights the need for asynchrony consideration when utilizing clustering techniques, e.g. depending on the processing followed of the received samples, 8 clusters may correspond to 2 (asynchronous) tags with time offset or 3 tags in perfect synchrony.

[3]Such sampling of $y_f[\cdot]$ offers exactly the values of Eq. (14) $\boldsymbol{y}_i$, according to its derivation in the appendix.

B. SNR calculation

Due to $\tau \neq 0$, it is shown below that the signal energy ratio between the two tags depends on that time offset parameter. The following definition is first presented:

Definition 1. *Based on Eq.* (8)*, the average received energy per bit for tag m, assuming FM0 encoding observed with a $T/2$ shift, is given by:*

$$\mathcal{E}_{bit}^m \triangleq \mathbb{E}\left[\mu_m^2 \left|h_m\right|^2 \int_0^T \left|x_m(t)\right|^2 dt\right] = \mu_m^2\, \mathbb{E}[|h_m|^2]\, \frac{T}{2}. \quad (16)$$

The following lemma is given for tag signal-to-noise ratio (SNR):

Lemma 1. *Based on Eqs.* (14)*,* (16)*, signal-to-noise ratio for tag a is given by:*

$$\mathit{SNR}_a \triangleq \frac{\mathbb{E}\left[\left|h_a \sqrt{\frac{\mathcal{E}_{bit}^a}{\mathbb{E}[|h_a|^2]}}\, \boldsymbol{x}_{a,i}\right|^2\right]}{\mathbb{E}[|\boldsymbol{n}_i|^2]} = \frac{\mathcal{E}_{bit}^a}{2N_0 W T_s}. \quad (17)$$

Proof. The numerator stems from straightforward calculation and the fact that $|\boldsymbol{x}_{a,i}| = |\boldsymbol{e}_0| = |\boldsymbol{e}_1| = 1$; the denominator calculation stems from Eq. (40). ■

Similarly, SNR for tag b follows:

Lemma 2. *Based on Eqs.* (14)*,* (16)*, tag b signal-to-noise ratio is given by:*

$$\begin{aligned}\mathit{SNR}_b &\triangleq \frac{\mathbb{E}\left[\left|\boldsymbol{B}_{(i-1,i)}\, h_b \sqrt{\frac{\mathcal{E}_{bit}^b}{\mathbb{E}[|h_b|^2]}}\, \boldsymbol{x}_{b,i}\right|^2\right]}{\mathbb{E}[|\boldsymbol{n}_i|^2]} \\ &= \begin{cases} \dfrac{\mathcal{E}_{bit}^b}{2N_0 W T_s}, & \text{if } \tau = 0, \\ \dfrac{\left(5L^2 - 12L\tau + 12\tau^2\right)\mathcal{E}_{bit}^b}{4N_0 W T_s L^2}, & \text{if } \tau > 0. \end{cases}\end{aligned} \quad (18)$$

Proof. For $\tau = 0$ the proof stems from Lemma 1. For $\tau > 0$ the proof is given in Appendix B. ■

The following power ratio will be also found useful in the numerical results; as in every multi-user setup, performance is dictated not only by SNR but also relative power among users/tags:

Definition 2. *The power ratio of tag a over b is defined as:*

$$\mathit{PR}_{ab} \triangleq \frac{\mathit{SNR}_a}{\mathit{SNR}_b}. \quad (19)$$

Finally, the following calculation will be needed in the link budget calculations and numerical results:

Lemma 3. *The 4-th moment of the Rician distribution is given by,*

$$\mathbb{E}[|h_m|^2] \triangleq \mathbb{E}[|h_{\mathrm{T}_m\mathrm{R}}|^4] = \frac{(\sigma^2_{h_{\mathrm{T}_m\mathrm{R}}})^2(\kappa_m^2 + 4\kappa_m + 2)}{(\kappa_m + 1)^2}. \quad (20)$$

Proof. The proof is given in Appendix C. ■

IV. Detection Techniques

This work exploits the transformation of Section III and processes the signal with a $T/2$ time-shift. Depending on the duration of the signal observed before detection, there are several detectors that can be tested, described below; $\hat{h}_m$ stands for $h_m\sqrt{\frac{\mathcal{E}_{bit}^m}{\mathbb{E}[|h_m|^2]}}$ for tag $m \in \{a, b\}$, which is either estimated or perfectly known; τ is assumed known through estimation; algorithms that estimate these parameters are offered next, in Section V.

A. T Detection for tag b

In the case of tag b detection, the detector that minimizes bit error rate (BER) of the received signal, utilizing a T-signal duration, is given by the minimum distance rule:

$$\hat{\boldsymbol{x}}_{a,i}, \hat{\boldsymbol{x}}_{b,i}, \hat{\boldsymbol{x}}_{b,i-1} = \\ = \underset{\substack{\boldsymbol{x}_{a,i},\\ \boldsymbol{x}_{b,i},\boldsymbol{x}_{b,i-1}}}{\operatorname{argmin}} \left\{ ||\boldsymbol{y}_i - \hat{h}_a\, \boldsymbol{x}_{a,i} - \boldsymbol{B}_{(i-1,i)}\, \hat{h}_b\, \boldsymbol{x}_{b,i}||_2^2 \right\}, \quad (21)$$

From Eq. (21), only bit information of tag b can be detected, through $\hat{\boldsymbol{x}}_{b,i}$ and $\hat{\boldsymbol{x}}_{b,i-1}$ and Eq. (12). However, this method is suboptimal since it does not utilize a $2T$ detection window, required for BER-optimal FM0 decoding.

B. $2T$ Detection for tag a

In the case of $2T$ tag a detection, the first T-block is used to detect $\hat{\boldsymbol{x}}_{a,i-1}$ and the second T-block is used to detect $\hat{\boldsymbol{x}}_{a,i}$; information from tag b is not detected jointly across the two consecutive T-blocks:

$$\hat{\boldsymbol{x}}_{a,i},\hat{\boldsymbol{x}}_{a,i-1} = \underset{\substack{\boldsymbol{x}_{a,i},\boldsymbol{x}_{a,i-1},\\ \boldsymbol{x}_{b,i},\boldsymbol{x}_{b,i-1},\boldsymbol{x}'_{b,i-1},\boldsymbol{x}_{b,i-2}}}{\operatorname{argmin}} \Big\{ ||\boldsymbol{y}_i - \hat{h}_a\, \boldsymbol{x}_{a,i} - \boldsymbol{B}_{(i-1,i)}\, \hat{h}_b\, \boldsymbol{x}_{b,i}||_2^2 \\ + ||\boldsymbol{y}_{i-1} - \hat{h}_a\, \boldsymbol{x}_{a,i-1} - \boldsymbol{B}_{(i-2,i-1)}\, \hat{h}_b\, \boldsymbol{x}'_{b,i-1}||_2^2 \Big\}. \quad (22)$$

Thereinafter, $\hat{\boldsymbol{x}}_{a,i}, \hat{\boldsymbol{x}}_{a,i-1}$ are used according to Eq. (12) to detect the information bit. However, the above also gives $\hat{\boldsymbol{x}}_{b,i-2}$, $\hat{\boldsymbol{x}}'_{b,i-1}$ from the first T-block and $\hat{\boldsymbol{x}}_{b,i-1}$, $\hat{\boldsymbol{x}}_{b,i}$ from the second T-block. Considering that $\hat{\boldsymbol{x}}'_{b,i-1} \neq \hat{\boldsymbol{x}}_{b,i-1}$ from one T-block to the other, this detector is suboptimal.

C. $2T$ Detection for tag a and tag b

In this case, both tags are jointly decoded using $2T$ signal observation:

$$\hat{\boldsymbol{x}}_{a,i}, \hat{\boldsymbol{x}}_{a,i-1}, \hat{\boldsymbol{x}}_{b,i}, \hat{\boldsymbol{x}}_{b,i-1}, \hat{\boldsymbol{x}}_{b,i-2} = \\ = \underset{\substack{\boldsymbol{x}_{a,i},\boldsymbol{x}_{a,i-1},\\ \boldsymbol{x}_{b,i},\boldsymbol{x}_{b,i-1},\boldsymbol{x}_{b,i-2}}}{\operatorname{argmin}} \Big\{ ||\boldsymbol{y}_i - \hat{h}_a\, \boldsymbol{x}_{a,i} - \boldsymbol{B}_{(i-1,i)}\, \hat{h}_b\, \boldsymbol{x}_{b,i}||_2^2 \\ + ||\boldsymbol{y}_{i-1} - \hat{h}_a\, \boldsymbol{x}_{a,i-1} - \boldsymbol{B}_{(i-2,i-1)}\, \hat{h}_b\, \boldsymbol{x}_{b,i-1}||_2^2 \Big\}. \quad (23)$$

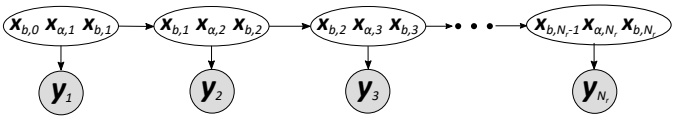

Fig. 5: Hidden Markov Model of the proposed signal model.

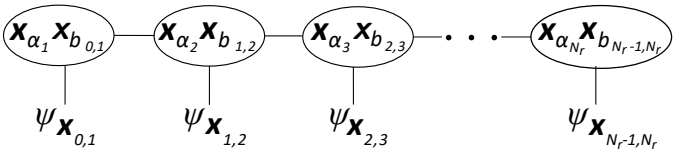

Fig. 6: Truncated probabilistic graphical model.

D. Viterbi

In the case of the Viterbi joint sequence detection, the proposed system model can be represented by the hidden Markov model (HMM) of Fig. 5, where the shaded and white nodes represent the observed random variables and the hidden states, respectively. Incorporating the observed data into the HMM, the truncated HMM of Fig. 6 is obtained, where $\psi_{\boldsymbol{x}_{a_i}\boldsymbol{x}_{b_{i-1,i}},\boldsymbol{y}_i} \triangleq \psi_{\boldsymbol{x}_{i-1,i}}$ denotes the resulting singleton potentials. To further ease notation, $\boldsymbol{x}_{b,i-1}\,\boldsymbol{x}_{b,i} \triangleq \boldsymbol{x}_{b_{i-1,i}}$.

The transition probabilities are defined as follows:

$$\mathbb{P}(\boldsymbol{x}_{a_2} = \boldsymbol{a}, \boldsymbol{x}_{b_{1,2}} = \boldsymbol{cd}\ |\boldsymbol{x}_{b_1} = \boldsymbol{b}) \triangleq \mathbb{1}(\boldsymbol{b} = \boldsymbol{c}), \quad (24)$$

$$\mathbb{P}(\boldsymbol{x}_{a_{i+1}} = \boldsymbol{a}, \boldsymbol{x}_{b_{i,i+1}} = \boldsymbol{df}\ |\boldsymbol{x}_{b_{i-1,i}} = \boldsymbol{bc}) \triangleq \mathbb{1}(\boldsymbol{c} = \boldsymbol{d}), \quad (25)$$

where $\boldsymbol{a}, \boldsymbol{b}, \boldsymbol{c}, \boldsymbol{d}, \boldsymbol{f}, \boldsymbol{g} \in \{\boldsymbol{e}_0, \boldsymbol{e}_1\}$, $\boldsymbol{x}_{b_{i,i+1}} = \boldsymbol{cd}$ stands for $\boldsymbol{x}_{b,i} = \boldsymbol{c}$, $\boldsymbol{x}_{b,i+1} = \boldsymbol{d}$ and $i \in \{1, 2, \ldots, \mathsf{N}_r - 1\}$ with $\mathsf{N}_r = 16$ denoting the number of bits in the RN16 packet. The above states that the allowed transitions are those where $\boldsymbol{x}_{b,i}$ of stage i is the same as $\boldsymbol{x}_{b,i}$ of stage $i+1$, as in Fig. 7.

The singleton potential functions are given by:

$$\psi_{\boldsymbol{x}_{i-1,i}}(\boldsymbol{a}, \boldsymbol{bc}) \propto \exp\left\{ -\frac{||\boldsymbol{y}_i - \hat{h}_a \boldsymbol{x}_{a,i} - \boldsymbol{B}_{(i-1,i)}\hat{h}_b \boldsymbol{x}_{b,i}||_2^2}{\sigma^2} \right\}, \quad (26)$$

where $\psi_{\boldsymbol{x}_{i-1,i}}(\boldsymbol{a}, \boldsymbol{bc}) = \psi(\boldsymbol{x}_{a,i} = \boldsymbol{a}, \boldsymbol{x}_{b_{i-1,i}} = \boldsymbol{cd}, \boldsymbol{y}_i)$ and $\boldsymbol{x}_{b_{i-1,i}}$ is encoded into the shaping matrix $\boldsymbol{B}_{(i-1,i)}$. In Eq. (26), for $i = 1$, $\boldsymbol{x}_{b,i-1} = \boldsymbol{x}_{b,0} = [1\ 0]^T$, where 1 is the last bit of the preamble sequence and 0 is the first bit of the FM0 line-coded RN16 sequence.

Since $\mathbb{P}(\boldsymbol{x}_{a_{i+1}} = \boldsymbol{a}, \boldsymbol{x}_{b_{i,i+1}} = \boldsymbol{df} | \boldsymbol{x}_{b_{i-1,i}} = \boldsymbol{bc}) = \mathbb{1}(\boldsymbol{c} = \boldsymbol{d})$, taking its logarithm results to either 0 or $-\infty$ and hence, we omit it in the following process but also keep in mind only the legal transitions. Using the Max-Sum message update equation the following is obtained:

$$\log m_{(i-1,i)\to(i,i+1)}(\boldsymbol{a}, \boldsymbol{df}) = \\ = \max_{\boldsymbol{g},\boldsymbol{b}} \left\{ \log\, \psi_{\boldsymbol{x}_{i-1,i}}(\boldsymbol{g}, \boldsymbol{bd}) + \log m_{(i-2,i-1)\to(i-1,i)}(\boldsymbol{g}, \boldsymbol{bd}) \right\} \\ = \max_{\boldsymbol{g},\boldsymbol{b}} \Big\{ -||\boldsymbol{y}_i - \hat{h}_a \boldsymbol{x}_{a,i} - \boldsymbol{B}_{(i-1,i)}\hat{h}_b \boldsymbol{x}_{b,i}||_2^2 \\ + \log m_{(i-2,i-1)\to(i-1,i)}(\boldsymbol{g}, \boldsymbol{bd}) \Big\}, \quad (27)$$

where $\boldsymbol{x}_{a,i+1} = \boldsymbol{a}$, $\boldsymbol{x}_{a,i} = \boldsymbol{g}$, $\boldsymbol{x}_{b,i+1} = \boldsymbol{f}$, $\boldsymbol{x}_{b,i} = \boldsymbol{d}$ and $\boldsymbol{x}_{b,i-1} = \boldsymbol{b}$.

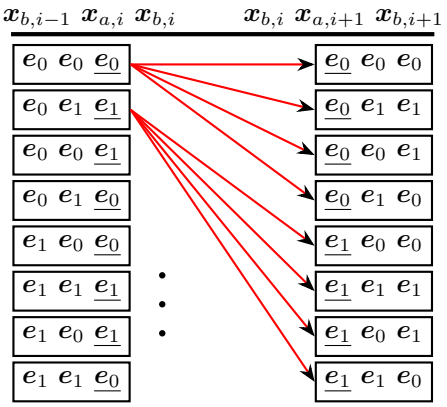

Fig. 7: Stages i and $i+1$ of the Viterbi trellis diagram.

In the forward pass of the Viterbi algorithm, the edge weights are calculated for each stage of the probabilistic graphical model (Figs. 6, 7), according to Eq. (27), while also keeping track of the node with the optimal weight, necessary for the backtracking process. In the backward pass of the algorithm, the path that sums to the optimal total weight is obtained, offering the optimal FM0 transmitted sequence both for tag a and tag b. The above setup can be visualized using the trellis diagram of Fig. 7.

Complexity of the Viterbi algorithm for a hidden Markov model (HMM) of a sequence of N hidden variables, each assuming $|X|$ discrete values, is given by $O(N|X|^2)$. Thus, the complexity of the joint sequence detection through Viterbi is given by $O(N(2^3)^2) = O(64\ N)$, according to Figs. 5, 6; N corresponds to the number of RN16 bits, and thus, $N = 16$.

E. Zero-Forcing

The single antenna zero-forcing (ZF) detector proposed in [5], treats one of the two tag responses as interference and projects the signal constellation into the subspace that completely cancels the interference, orthogonal to the interfering component:

$$\boldsymbol{s}_a[k] = \left[\boldsymbol{I}_2 - \frac{\boldsymbol{h}_b \boldsymbol{h}_b^T}{\boldsymbol{h}_b^T \boldsymbol{h}_b}\right] \boldsymbol{s}[k],\ \boldsymbol{s}_b[k] = \left[\boldsymbol{I}_2 - \frac{\boldsymbol{h}_a \boldsymbol{h}_a^T}{\boldsymbol{h}_a^T \boldsymbol{h}_a}\right] \boldsymbol{s}[k], \quad (28)$$

where $\boldsymbol{h}_a = [\Re\{\hat{h}_a\}\ \Im\{\hat{h}_a\}]^T$, $\boldsymbol{h}_b = [\Re\{\hat{h}_b\}\ \Im\{\hat{h}_b\}]^T$, $\boldsymbol{s}[k] = [\Re\{y_f[k]\}\ \Im\{y_f[k]\}]^T$ and $y_f[k]$ is according to Eq. (13). The projection $\boldsymbol{s}_m$ of each tag signal is thereafter decoded separately. It must be noted that this receiver is capable of resolving a collision from *strictly* two tags participating, since a subspace cannot be found in the two-dimensional I/Q plane, which is orthogonal to more than one interferer.

V. Digital Link Housekeeping

A. DC Estimation

The DC offset can be estimated in time periods where all tags remain silent. In Gen2 applications, the DC offset is estimated by averaging the received samples acquired from the signal part right after the QUERY command has been sent from the reader, up to the point before the tags start switching, defined as interval T_1 [1]. The estimated offset is then subtracted from each sample, offering Eq. (8).

B. Channel Estimation

The algorithm used to estimate the channel coefficients follows work in [4]. In order to obtain the channel estimates, the received samples are projected onto the subspace defined by the DC component and the $h_a + h_b$ cluster. The $\widehat{h_a + h_b}$ estimate can be obtained either from the end or from the start of the preamble packet, defined as $\boldsymbol{s}_p = [1\ 1\ 0\ 1\ 0\ 0\ 1\ 0\ 0\ 0\ 1\ 1]$ in [1], for a single tag. At these positions there are two consecutive data-1 bits, so even after the observed shifting due to the delayed response of tag b, the upsampled (by L) superimposed sequences will still have overlapping data-1 bits, offering an estimate for $h_a + h_b$.

The algorithm is based on the observation that two states (out of the possible 4, 6 or 8, see Sec. III-A), are realized during the transmission of the RN16 packet preamble (due to common information transmission from the two tags, assuming synchrony), defining an one-dimensional subspace s_x (i.e., a line). Projecting the received samples of the RN16 packet onto the subspace orthogonal to s_x, will give a non-zero value if the corresponding half-bit is equal to h_a or h_b. The algorithm searches for points that have the maximum signal strength in this orthogonal subspace. More specifically, the received waveform is processed with matched filtering, offering y_f, and the maximum signal strength indices and corresponding channel coefficients, are estimated as follows:

$$k_A = \underset{k\in\{0,\ldots,\mathsf{N}L\}}{\operatorname{argmax}} \Im\left\{y_f[k] e^{-j\widehat{\angle h_a + h_b}}\right\}, \quad (29)$$

$$k_B = \underset{k\in\{0,\ldots,\mathsf{N}L\}}{\operatorname{argmin}} \Im\left\{y_f[k] e^{-j\widehat{\angle h_a + h_b}}\right\}, \quad (30)$$

$$\hat{h}_a = y_f[k_A], \quad \hat{h}_b = y_f[k_B], \quad (31)$$

where $\mathsf{N} = \mathsf{N}_p + \mathsf{N}_r$ is the total number of transmitted bits (preamble + RN16). It is important to ensure that the estimates $\hat{h}_a$ and $\hat{h}_b$ are correctly assigned to each tag or if they need to be swapped, otherwise the performance of the detection methods will not be optimal. In order to check that $\hat{h}_a$ indeed corresponds to tag a and $\hat{h}_b$ to tag b, a mean squared error metric is utilized in this work, detailed in Sec. V-C, below.

Even though this algorithm was initially developed for values of $\tau < L/10$, it still works in this problem formulation, as will be shown in the numerical results section; that is due to the fact that the projection of all samples will always be closer to the subspace s_x than the samples corresponding to h_a and h_b, no matter the value of τ or the number of clusters it produces on the I/Q plane.

C. Time Offset Estimation

Time offset τ estimation is based on channel state information (CSI) estimation. By the problem's definition tag a responds first ($\tau_a = 0$); thus, the detected packet start of the collided RN16 sequence, is also the start of tag a response. In order to detect the RN16 packet start, a correlation-based method is utilized with the (known) preamble bits of RN16.

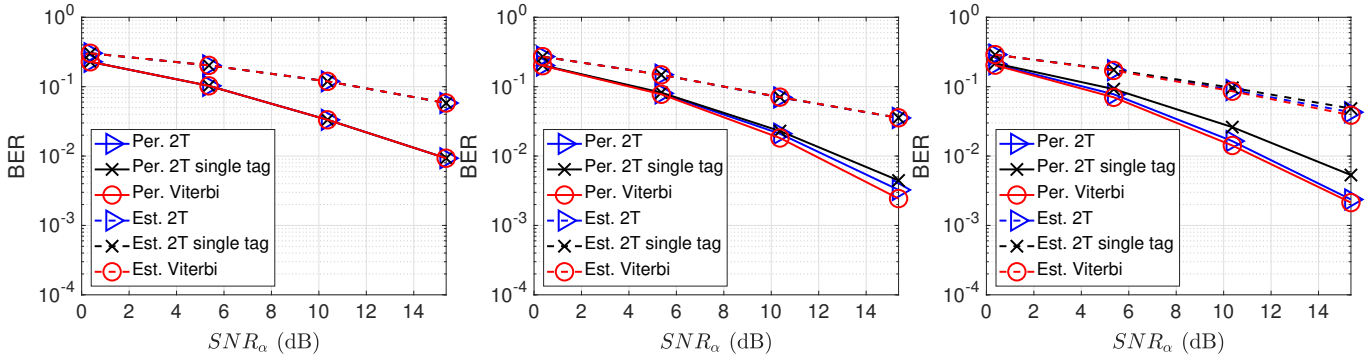

(a) $\tau = 0$, $\text{PR}_{ab} = 2.24$ dB. (b) $\tau = 10$, $\text{PR}_{ab} = 0.36$ dB. (c) $\tau = 25$, $\text{PR}_{ab} = 2.2423$ dB.

Fig. 8: Tag a BER evaluation at $d_a = 7.5$ m, $d_b = 8.0$ m.

The time offset estimation algorithm is based upon creating the discrete channel equivalent, which basically is an ideal superposition of the two tags preamble bits sequences for different values of τ and comparing it, using the minimum distance rule, to the received samples of the preamble part of the packet. An estimate for τ is thus obtained by minimizing the following mean squared error (MSE):

$$\hat{\tau} = \underset{\tau \in \{0,1,\ldots,L-1\}}{\text{argmin}} \frac{1}{K} \sum_{k=0}^{K-1} \left| y_f[k] - c_f[k] \right|^2, \qquad (32)$$

where $K = \mathsf{N}_p L$, $\mathsf{N}_p = 6$ the number of preamble bits and $c_f[k]$ the output of the matched filtering process, with

a square pulse $\Pi[k]$ of length $L/2$, on the discrete channel equivalent $c[k]$; the latter is defined as follows:

$$c[k] = \hat{h}_a \, \boldsymbol{s}_{p,\text{up}} + \hat{h}_b \, [\underbrace{0 \ldots 0 \; 0}_{\tau} \; \boldsymbol{s}_{p,\text{up}}], \qquad (33)$$

$$c_f[n] = \sum_{k=-\infty}^{\infty} c[k] \Pi[n-k], \qquad (34)$$

where $\boldsymbol{s}_{p,\text{up}}$ denotes the upsampled, by a factor of L, preamble bits sequence. Notice that $c_f[n]$ above requires estimates of the channels $\hat{h}_a$, $\hat{h}_b$.

In order to check whether the channel estimates are correctly assigned to each tag, the above time offset algorithm must be run twice, once with $\hat{h}_a$ corresponding to tag a and $\hat{h}_b$ to tag b and once more where the mapping is *swapped*. The channel estimates are then accordingly mapped, depending on which of the two runs returned the minimum MSE.

VI. Numerical Results

Figs. 8, 9, 10 are offered with $\mathsf{N}_p = 6$ preamble and $\mathsf{N}_r = 16$ payload bits. 10^4 Monte Carlo runs were performed per SNR value, while channel parameters remained constant for each run. The rest of the parameters follow: $f_c = 868$ MHz, BLF $= 40$ kHz, $F_s \triangleq 1/T_s = 2$ MHz, $L = T/T_s \equiv F_s/\text{BLF} = 50$, $T = 1/\text{BLF} = 25$ μs, $\kappa_a = 10$, $\kappa_b = 9$, $v_a = v_b = 4$,

$\Gamma_0 = 0$, $\Gamma_1 = 1$, $\eta = 10\%$ and P_c ranging from 15 to 30 dBm. Different operating regimes of the detectors are evaluated, since the tag-to-reader distances are altered from $d_a = 7.5$ m and $d_b = 8.0$ m in Fig. 8, to $d_a = 8.5$ m and $d_b = 7.6$ m in Fig. 10, offering different tag power ratio (PR_{ab} or PR_{ba} according to Eq. (19)). Results will be presented assuming perfect CSI and τ estimation (ideal case), as well as estimated CSI and τ (practical case), according to the algorithms presented in Sec. V.

Fig. 8a depicts the synchronous case, i.e., $\tau = 0$, where the $2T$ detectors (both tags or tag a) offer the same performance with the Viterbi, as expected; FM0 induced memory within two symbol periods is adequate for detection [21] and thus, longer memory - exploited in Viterbi - is not needed. The same plot depicts detection performance with perfect (ideal) knowledge of CSI, as well as performance with estimated CSI.

Detectors' performance does not coincide in the asynchronous case, in Figs. 8b, 8c, where $\tau = 10$, $\tau = 25$, respectively. The performance gap of the $2T$ detectors compared to Viterbi in the asynchronous case is due to the extra induced memory from the delayed tag b; such delay requires detection of information from additional symbols (compared to the synchronous case), rendering the $2T$ detectors suboptimal. The same plots also depict results with perfect knowledge of the channels, as well as estimated channels. In the asynchronous case, the $2T$ detection of both tags outperforms the $2T$ detection of (single) tag a only, as expected. At the high SNR regime, in the order of 15 dB, offered BER with estimated (perfect) channel is in the order of 3% (0.4%) and thus, the expected number of erroneously detected RN16 bits is strictly less than 1. The latter clearly shows that RN16 tag collision is not an issue for the specific detectors. Moreover, the value of τ in the detectors' performance is important and presents an oscillating behaviour; BER is not monotonically increasing (or decreasing) as a function of τ.

Fig. 9 compares performance of the zero-forcing, the joint $2T$ and the Viterbi detector for tag a, under perfect CSI, with the same simulation parameters as Fig. 8b. It can be clearly observed that both $2T$ and the Viterbi detector outperform the ZF detector; that is expected since the latter does not initially take into account asynchrony, i.e., the time offset between the two tags, before the projection is performed. Thus, it is important to employ detection techniques that explicitly take into account asynchronous operation of tags, which is not

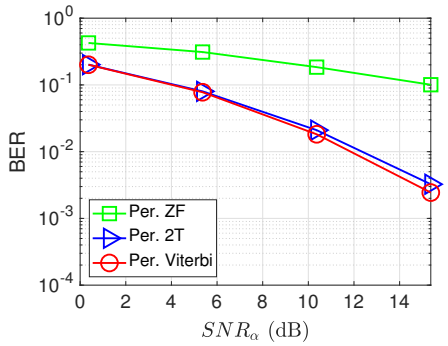

Fig. 9: Tag a BER evaluation at $\tau = 10$.

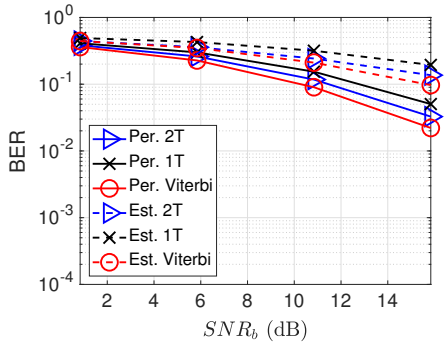

(a) $\tau = 35$, $\text{PR}_{ba} = 4.82$ dB.

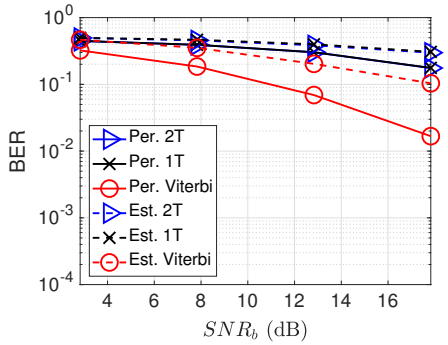

(b) $\tau = 45$, $\text{PR}_{ba} = 6.81$ dB.

Fig. 10: Tag b BER evaluation at $d_a = 8.5$ m, $d_b = 7.6$ m.

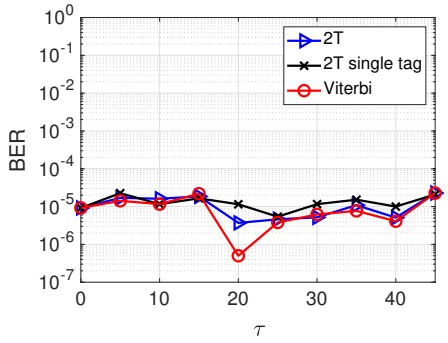

Fig. 11: Delay offset impact on BER of tag a.

uncommon in commercial RFID systems.

Figs. 10a, 10b demonstrate the performance of the $1T$, joint $2T$ and the Viterbi detectors for tag b data detection in the asynchronous case, where $\tau = 35$ and $\tau = 45$, respectively, when tag b signal is stronger than tag a. The oscillating BER behaviour of Fig. 8 is once again observed in both Figs. 10a, 10b, while the performance gap between Viterbi and the $1T$, joint $2T$ detectors is clearly more notable in Fig. 10b, for $\tau = 45$. At the high SNR regime around 16 dB, BER with estimated (perfect) channel is in the order of 10% (2%); 10% BER does not suffice for zero-error RN16 detection of tag b. Thus, it is important for the reader to flip the roles between tag a and b, and treat the stronger signal as tag a. However, that requires more research on packet synchronization techniques, that could lock to the stronger packet/tag, irrespectively of the delay among the two tags. It is noted that the literature typically offers packet synchronization techniques that lock on the packet that arrives first (e.g., work in [22]).

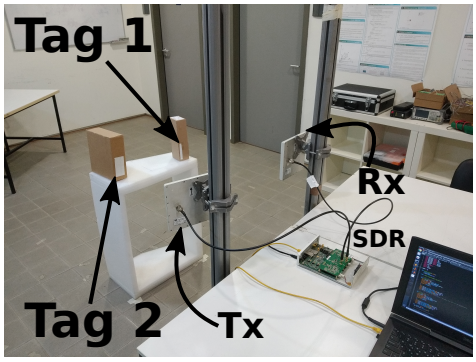

Fig. 12: Experimental setup with SDR implementation of Gen2. The anti-collision algorithm was implemented in C++.

Fig. 11 demonstrates detection performance for different delay values, under estimated CSI. The parameters used in this simulation are as follows: $P_c = 20$ dBm, $d_a = d_b = 0.6$ m, $f_c = 900$ MHz, $F_s = 20$ MHz, BLF $= 100$ kHz, $\eta = 0.1$, and $v_a = v_b = 2$, while 10^5 Monte Carlo runs were conducted.[4] Under perfect CSI, the observed BER was found equal to BER $= 0$, while under estimated CSI, the observed BER was found less than 10^{-4}, for any value of τ. It is noted that under similar conditions, prior art algorithms in [14], offered BER in the order of BER $\geq 10^{-4}$.

A. Experimental Results with Software-Defined Radio (SDR)

The algorithm was developed in C++ and added in the open-source Gen2 software stack developed in [2]. In all experiments, 2 Gen2 UHF RFID tags (1 ALN-9840-WRW and 1 ZEBRA 4"×2" Z-PERFORM 1500T) were attached to empty boxes, at various distances away for the reader antennas, as shown in Fig. 12. The experimental setup included a USRP N200 with an RFX900 daughterboard and two circularly-polarized MTI MT-242032 antennas (one for Tx and one for Rx) with a gain of 7 dBic each. A spectrum analyzer was used to measure the received signal strength indicator (RSSI) at the location of the tags and at the carrier frequency of 868 MHz at which the whole system operated. A 24 dB Mini-Circuits

[4]Decimation factor of 4 was also utilized, reducing to $L = 50$ from nominal $L = 200$.

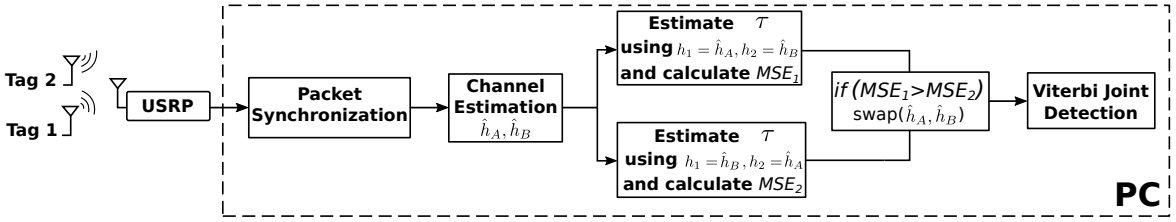

Fig. 13: Block diagram of the collision resolution process.

TABLE III: Experimental performance evaluation.

	80 cm	130 cm	280 cm (with Amplifier)	300 cm (with Amplifier)
Measured RSSI	-9.5 dBm	-11.9 dBm	-15.8 dBm	-14.5 dBm
Single Tag Detection	28.55%	25.80%	25.30%	11.85%
This work	43.25%	33.80%	33.20%	22.40%

ZRL-1200+ amplifier was also exploited in addition to a 9 dB attenuator between the amplifier and the RFX daughterboard. The software was executed in a laptop computer. Number of slots per round was set equal to 1, in order to force the collision. The total number of inventory rounds was set to 2000 in each experiment and various levels of distances and respective RSSI were tested. DC cancellation, channel estimation, time offset estimation and packet synchronization were implemented, as described in Section V; the whole process followed is visualized at the block diagram of Fig. 13.

Since commercial RFID tags were used, their RN16 information is randomized and thus, not a priori known. In order to make sure that the algorithm correctly detected RN16, the following approach was used: a tag will respond with its EPC information only if the reader acknowledges its correct RN16. Since, collision resolution is executed at the reader, correct detection of tag RN16 information at the SDR reader will be escorted with EPC transmission from a tag. The algorithm detects the two tags RN16 information and reports back the RN16 of tag a, i.e., the first tag that responded. The reader acknowledges back the detected RN16 and a tag reports back only if the RN16 reported by the reader was the information that the tag transmitted.

Table III shows the experimental results. For 80 cm distance between reader antennas and tags, the single tag detection algorithm offered successful tag interrogation around 560 times out of 2000 (corresponding to 28.55% success rate); in contrast, the collision resolution method of this work increased the successful interrogations to around865 times out of 2000 (corresponding to 43.25% success rate). It is noted that single tag detection is utilized in SIC-based techniques, which are more appropriate for multi-user scenarios with significant differences among the users' received signal power. Performance gains around 10% were observed for other communication distances, with or without the amplifier. Such performance gains in the order of 10% increase the reading rate of any commercial RFID reader by that amount, without any hardware modifications and thus, may be of great commercial value. It was also observed during the experiments that the tags' RF energy harvesting and backscattering operation was affected in a non-linear way by distance and amplification gain, as expected; such behavior will be further studied in future work.

VII. Conclusion

It was clearly shown that the proposed detectors leveraging the closed form signal model, demonstrated robust performance in a 2-tags collision scenario. It was demonstrated for the first time, that even though the performance gap between the joint $2T$ and the Viterbi detector is small, the joint $2T$ detector is not the optimal detector in this case, since there is extra memory induced due to the delayed response of the second tag. Furthermore, it was shown that the joint $2T$ and the Viterbi joint sequence detector coincide in the synchronous 2-tags case. It was also found that the offered BER of the detectors does not present a monotonic behavior but rather oscillates for different delay values. Asynchronous detection has been overlooked in classic digital communications; in the era of batteryless, ultra-low cost tags, more work is clearly needed. Future research will focus on channel estimation and packet synchronization when more than 2 tags collide, as well as the integration of the Miller line coding scheme.

Appendix A
Proof of Theorem 1

Sampling Eq. (8) by T_s, the following is obtained:

$$\tilde{y}[k] \triangleq \tilde{y}(kT_s) = h_a\,\mu_a\,x_a[k] + h_b\,\mu_b\,x_b[k] + n[k], \quad (35)$$

where $x_a[k] \triangleq x_a(kT_s)$, $x_b[k] \triangleq x_b(kT_s) \in \{0,1\}$ and $n[k] \triangleq n(kT_s)$ Gaussian process with

$$\mathbb{E}[|n(kT_s)|^2] = \int_{-W}^{W} S_{nn}(F)\,dF = \frac{N_0}{2}2W = N_0W. \quad (36)$$

Thus, $n[k] \sim \mathcal{CN}(0, \underbrace{N_0W}_{2\sigma_n^2}) \equiv \mathcal{CN}(0, 2\sigma_n^2)$.

The discrete baseband equivalent signal over a half-bit duration $T/2$, using matched filtering with rectangular pulse, for $j=0$ for the first half-bit and $j=1$ for the second half-bit, is obtained as follows:

$$y_j = T_s \sum_{k\in\mathcal{K}_j} \tilde{y}[k] \frac{1}{\sqrt{\frac{LT_s}{2}}} = \sqrt{\frac{2T_s}{L}} \sum_{k\in\mathcal{K}_j} \tilde{y}[k]$$
$$= \sqrt{\frac{2T_s}{L}} \left(\sum_{k\in\mathcal{K}_j} h_a\,\mu_a\,x_a[k] + h_b\,\mu_b\,x_b[k] \right) + n_j, \quad (37)$$

where $1/\sqrt{LT_s/2}$ is the appropriate normalization factor for unit energy, corresponding to orthonormal basis functions for expansion of the received signal with duration T, $j \in \{0,1\}$ and $\mathcal{K}_0 = \{0,1,\ldots,L/2-1\}$, $\mathcal{K}_1 = \{L/2, L/2+1,\ldots,L-1\}$.

Each FM0 symbol observed with a $T/2$ shift can be written as a 2×1 complex vector $\boldsymbol{y}_i = [y_0^i \; y_1^i]^T$, where i denotes the i-th received T-duration symbol. With tag a perfectly synced to the detection window, one can only observe waveforms $S_0(t)$ or $S_1(t)$ for tag a; however, the same does not hold for tag b. Depending on the delay of tag b RN16 response, a perfect $S_0(t)$ or $S_1(t)$ waveform might never be observed in the detection window, but rather a shifted combination of the two.

First, $\tau < L/2$ is assumed, as in the example of Fig. 4, where tag a is emitting $S_0(t)$ waveform, which corresponds to $\boldsymbol{x}_{a,i} = \boldsymbol{e}_0$; tag b backscatters $S_1(t)$, delayed by τ samples, corresponding to $\boldsymbol{x}_{b,i} = \boldsymbol{e}_1$. Immediately before that, tag b backscatters $S_1(t)$, which corresponds to $\boldsymbol{x}_{b,i-1} = \boldsymbol{e}_1$. Thus, according to Eq. (37) and the definition of $\boldsymbol{y}_i$, the following vector form is obtained for the specific signals of Fig. 4:

$$\begin{aligned}\boldsymbol{y}_i &= \begin{bmatrix} \sqrt{\frac{2T_s}{L}}\, h_a\, \mu_a\, \frac{L}{2}\cdot 1 + \sqrt{\frac{2T_s}{L}}\, h_b\, \mu_b\, \tau \cdot 1 + n_0^i \\ \sqrt{\frac{2T_s}{L}}\, h_a \mu_a\, \frac{L}{2}\cdot 0 + \sqrt{\frac{2T_s}{L}}\, h_b \mu_b \left(\frac{L}{2}-\tau\right)\cdot 1 + n_1^i \end{bmatrix} \\ &= \begin{bmatrix} \sqrt{\frac{2T_s}{L}}\, h_a\, \mu_a\, \frac{L}{2}\cdot 1 + \sqrt{\frac{2T_s}{L}}\, h_b\, \mu_b\, \frac{L}{2}\left(\frac{2\tau}{L}\right)\cdot 1 + n_0^i \\ \sqrt{\frac{2T_s}{L}}\, h_a\, \mu_a\, \frac{L}{2}\cdot 0 + \sqrt{\frac{2T_s}{L}}\, h_b\, \mu_b\, \frac{L}{2}\left(1-\frac{2\tau}{L}\right)\cdot 1 + n_1^i \end{bmatrix} \\ &= h_a\, \mu_a \sqrt{\frac{T}{2}} \begin{bmatrix}1\\0\end{bmatrix} + \underbrace{\begin{bmatrix} 0 & \frac{2\tau}{L} \\ 0 & 1-\frac{2\tau}{L}\end{bmatrix}}_{\boldsymbol{B}_{(i-1,i)}} h_b\, \mu_b \sqrt{\frac{T}{2}} \begin{bmatrix}0\\1\end{bmatrix} + \begin{bmatrix} n_0^i \\ n_1^i \end{bmatrix},\end{aligned} \tag{38}$$

where

$$n_j^i = \sqrt{\frac{2T_s}{L}} \sum_{k\in\mathcal{K}_j} n[k] \sim \mathcal{CN}\left(0, \underbrace{2\sigma_n^2 \left(\sqrt{\frac{2T_s}{L}}\right)^2 \frac{L}{2}}_{N_0 W T_s}\right), \tag{39}$$

and hence,

$$\boldsymbol{n}_i = \left[n_0^i \; n_1^i\right]^T \sim \mathcal{CN}\left(\boldsymbol{0}_2, N_0 W T_s \boldsymbol{I}_2\right). \tag{40}$$

Repeating the process above, for every scenario in Table II for $\tau < L/2$ and once more for $\tau \geq L/2$, while maintaining $\boldsymbol{x}_a$ in perfect sync to the detection window, yields the closed form of $\boldsymbol{B}_{(i-1,i)}$ matrices offered in Table I and eventually, Eq. (14).

It is noted that, since $n(t)$ is a circularly symmetric, complex baseband Gaussian random process with PSD $N_0/2$ in the $[-W;W]$ frequency band, its projections on an orthonormal basis (with basis functions limited in the $[-W;W]$ frequency band) will have independent and identically distributed (i.i.d.) circularly symmetric, complex Gaussian components with variance $N_0/2$, [23, pp. 213].

APPENDIX B
PROOF OF EQ. (18)

The expression of SNR_b for $\tau > 0$ is calculated as follows:

$$\begin{aligned}\text{SNR}_b &\triangleq \frac{\mathbb{E}\left[\left|\boldsymbol{B}_{(i-1,i)}\, h_b \sqrt{\frac{\mathcal{E}_{bit}^b}{\mathbb{E}[|h_b|^2]}}\, \boldsymbol{x}_{b,i}\right|^2\right]}{\mathbb{E}[|\boldsymbol{n}_i|^2]} \\ &= \frac{\mathbb{E}\left[\boldsymbol{x}_{b,i}^T \boldsymbol{B}^T \boldsymbol{B} \boldsymbol{x}_{b,i}\right] \mathcal{E}_{bit}^b}{2N_0 W T_s},\end{aligned} \tag{41}$$

where

$$\begin{aligned}\mathbb{E}\left[\boldsymbol{x}_{b,i}^T \boldsymbol{B}^T \boldsymbol{B} \boldsymbol{x}_{b,i}\right] &= \mathbb{E}_{\boldsymbol{x}_{b,i}}\Big\{ \underbrace{\mathbb{E}_{\boldsymbol{B}|\boldsymbol{x}_{b,i}}[\boldsymbol{x}_{b,i}^T \boldsymbol{B}^T \boldsymbol{B} \boldsymbol{x}_{b,i}]}_{g(\boldsymbol{x}_{b,i})} \Big\} \\ &= \frac{1}{2} g\left(\boldsymbol{x}_{b,i} = \begin{bmatrix}1\\0\end{bmatrix}\right) + \frac{1}{2} g\left(\boldsymbol{x}_{b,i} = \begin{bmatrix}0\\1\end{bmatrix}\right) \\ &= \frac{1}{2}[0 \quad 1]\mathbb{E}\left\{\boldsymbol{B}^T\boldsymbol{B}|\boldsymbol{x}_{b,i} = \begin{bmatrix}0\\1\end{bmatrix}\right\}\begin{bmatrix}0\\1\end{bmatrix} \\ &\quad + \frac{1}{2}[1 \quad 0]\mathbb{E}\left\{\boldsymbol{B}^T\boldsymbol{B}|\boldsymbol{x}_{b,i} = \begin{bmatrix}1\\0\end{bmatrix}\right\}\begin{bmatrix}1\\0\end{bmatrix}.\end{aligned} \tag{42}$$

$\mathbb{E}[\boldsymbol{B}^T\boldsymbol{B}|\boldsymbol{x}_{b,i}]$ in Eq. (42) is calculated as follows:

$$\mathbb{E}[\boldsymbol{B}^T\boldsymbol{B}|\boldsymbol{x}_{b,i}] = \sum_{\boldsymbol{B}^T\boldsymbol{B}} \frac{1}{4}\boldsymbol{B}^T\boldsymbol{B}. \tag{43}$$

For $\boldsymbol{x}_{b,i} = [1 \quad 0]^T$, according to Table I,

$$\begin{aligned}\sum_{\boldsymbol{B}^T\boldsymbol{B}} \frac{1}{4}\boldsymbol{B}^T\boldsymbol{B} &= \frac{1}{4}\left(\underbrace{\boldsymbol{B}_1^T\boldsymbol{B}_1 + \boldsymbol{B}_3^T\boldsymbol{B}_3}_{\tau<L/2} + \underbrace{\boldsymbol{B}_1^T\boldsymbol{B}_1 + \boldsymbol{B}_3^T\boldsymbol{B}_3}_{\tau\geq L/2}\right) \\ &= \frac{1}{4}\begin{bmatrix}\frac{12L^2-24\tau L+24\tau^2}{L^2} & 0 \\ 0 & 0\end{bmatrix}.\end{aligned} \tag{44}$$

Notice that the two $\boldsymbol{B}_j^T\boldsymbol{B}_j$ products are for a different range of τ values.

For $\boldsymbol{x}_{b,i} = [0 \quad 1]^T$ and according to Table I in the same fashion,

$$\begin{aligned}\sum_{\boldsymbol{B}^T\boldsymbol{B}} \frac{1}{4}\boldsymbol{B}^T\boldsymbol{B} &= \frac{1}{4}\left(\underbrace{\boldsymbol{B}_2^T\boldsymbol{B}_2 + \boldsymbol{B}_4^T\boldsymbol{B}_4}_{\tau<L/2} + \underbrace{\boldsymbol{B}_2^T\boldsymbol{B}_2 + \boldsymbol{B}_4^T\boldsymbol{B}_4}_{\tau\geq L/2}\right) \\ &= \frac{1}{4}\begin{bmatrix}0 & 0 \\ 0 & \frac{8L^2-24\tau L+24\tau^2}{L^2}\end{bmatrix}.\end{aligned} \tag{45}$$

Substituting Eqs. (44) and (45) into Eq. (42) we obtain:

$$\begin{aligned}\mathbb{E}[\boldsymbol{x}_{b,i}^T\boldsymbol{B}^T\boldsymbol{B}\boldsymbol{x}_{b,i}] &= \frac{1}{2}[1 \quad 0]\frac{1}{4}\begin{bmatrix}\frac{12L^2-24\tau L+24\tau^2}{L^2} & 0 \\ 0 & 0\end{bmatrix}\begin{bmatrix}1\\0\end{bmatrix} \\ &\quad + \frac{1}{2}[0 \quad 1]\frac{1}{4}\begin{bmatrix}0 & 0 \\ 0 & \frac{8L^2-24\tau L+24\tau^2}{L^2}\end{bmatrix}\begin{bmatrix}0\\1\end{bmatrix} \\ &= \frac{\frac{5}{2}L^2 - 6L\tau + 6\tau^2}{L^2}.\end{aligned} \tag{46}$$

Eventually, substituting Eq. (46) into Eq. (41) we obtain:

$$\text{SNR}_b = \frac{\left(5L^2 - 12\tau L + 12\tau^2\right)\mathcal{E}_{bit}^b}{4N_0 W T_s L^2}. \tag{47}$$

APPENDIX C
PROOF OF EQ. (20)

The baseband complex channel coefficients $h_{\mathrm{T}_a\mathrm{R}}$ and $h_{\mathrm{T}_b\mathrm{R}}$ are independent random variables following the Rician distribution according to [17], with parameters $\kappa_m = \frac{s^2}{2\sigma_g^2}$, where $s^2 = \frac{\rho\,\kappa_m}{\kappa_m+1}$, $2\sigma_g^2 = \frac{\rho}{\kappa_m+1}$ and $\rho \equiv \sigma^2_{h_{\mathrm{T}_m\mathrm{R}}}$. According to [24, Eq. (50)], the k-th moment of the Rician (Nakagami-n) distribution is calculated as follows:

$$\begin{aligned}
&\mathbb{E}[|h_{\mathrm{T}_m\mathrm{R}}|^k] \triangleq (2\sigma_g^2)^{k/2}\,\Gamma\left(1+\frac{k}{2}\right)\,{}_1F_1\left(-\frac{k}{2};1;-\frac{s^2}{2\sigma_g^2}\right)\\
&\overset{k=4}{=} 4\sigma_g^4\,\Gamma(3)\,{}_1F_1\left(-2;1;-\frac{s^2}{2\sigma_g^2}\right) = 8\sigma_g^4\left(1+\frac{s^2}{\sigma_g^2}+\frac{s^4}{8\sigma_g^4}\right)\\
&= 8\sigma_g^4 + 8\sigma_g^2 s^2 + s^4 = 2(2\sigma_g^2)^2 + 4(2\sigma_g^2)s^2 + s^4\\
&= 2\left(\frac{\rho}{\kappa_m+1}\right)^2 + 4\left(\frac{\rho}{\kappa_m+1}\right)s^2 + s^4\\
&= 2\left(\frac{\rho}{\kappa_m+1}\right)^2 + 4\left(\frac{\rho}{\kappa_m+1}\right)^2 + \left(\frac{\rho\,\kappa_m}{\kappa_m+1}\right)^2\\
&= \frac{\rho^2\left(\kappa_m^2+4\kappa_m+2\right)}{(\kappa_m+1)^2} = \frac{\left(\sigma^2_{h_{\mathrm{T}_m\mathrm{R}}}\right)^2\left(\kappa_m^2+4\kappa_m+2\right)}{(\kappa_m+1)^2},
\end{aligned} \tag{48}$$

where ${}_1F_1(\cdot)$ denotes the confluent hypergeometric function.

REFERENCES

[1] "EPC Radio-Frequency Identity Protocols, Class-1 Generation-2 UHF RFID Protocol for Communications at 860 MHz - 960 MHz, version 1.2.0 EPC Global," 2008.

[2] N. Kargas, F. Mavromatis, and A. Bletsas, "Fully-coherent reader with commodity SDR for Gen2 FM0 and computational RFID," *IEEE Wireless Commun. Lett.*, vol. 4, no. 6, pp. 617–620, Dec. 2015.

[3] D. Shen, G. Woo, D. P. Reed, A. B. Lippman, and J. Wang, "Separation of multiple passive RFID signals using software defined radio," in *Proc. IEEE Int. Conf. on RFID*, Orlando, FL, Apr. 2009, pp. 139–146.

[4] C. Angerer, G. Maier, M. V. Delgado, M. Rupp, and J. V. Alonso, "Single antenna physical layer collision recover receivers for RFID readers," in *Proc. IEEE Int. Conf. on Industrial Technology (ICIT)*, Vina del Mar, Chile, Mar. 2010, pp. 1406–1411.

[5] C. Angerer, R. Langwieser, and M. Rupp, "RFID reader receivers for physical layer collision recovery," *IEEE Trans. Commun.*, vol. 58, no. 12, pp. 3526–3537, Dec. 2010.

[6] J. Kaitovic, R. Langwieser, and M. Rupp, "RFID reader with multi antenna physical layer collision recovery receivers," in *Proc. IEEE Int. Conf. on RFID-Technologies and Applications (RFID-TA)*, Sep. 2011, pp. 286–291.

[7] J. Kaitovic, R. Langwieser, and M. Rupp, "A smart collision recovery receiver for RFIDs," *EURASIP Journal on Embedded Systems*, vol. 2013, no. 7, pp. 1–19, Apr. 2013.

[8] K. Fyhn, R. M. Jacobsen, P. Popovski, A. Scaglione, and T. Larsen, "Multipacket reception of passive UHF RFID tags: a communication theoretic approach," *IEEE Trans. Signal Processing*, vol. 59, no. 9, pp. 4225–4237, Sep. 2011.

[9] J. Wang, H. Hassanieh, D. Katabi, and P. Indyk, "Efficient and reliable low-power backscatter networks," in *Proc. ACM SIGCOMM*, Helsinki, Finland, Aug. 2012, pp. 61–72.

[10] G. Vannucci, A. Bletsas, and D. Leigh, "A software-defined radio system for backscatter sensor networks," *IEEE Trans. Wireless Commun.*, vol. 7, no. 6, pp. 2170–2179, Jun. 2008.

[11] P. Hu, P. Zhang, and D. Ganesan, "Leveraging interleaved signal edges for concurrent backscatter," *SIGMOBILE Mob. Comput. Commun. Rev.*, vol. 18, no. 3, pp. 26–31, Jan. 2015.

[12] ——, "Laissez-faire: Fully asymmetric backscatter communication," *SIGCOMM Comput. Commun. Rev.*, vol. 45, no. 4, pp. 255–267, Aug. 2015.

[13] J. Ou, M. Li, and Y. Zheng, "Come and be served: Parallel decoding for COTS RFID tags," *IEEE/ACM Trans. Netw.*, vol. 25, no. 3, pp. 1569–1581, Jun. 2017.

[14] M. Jin, Y. He, X. Meng, Y. Zheng, D. Fang, and X. Chen, "FlipTracer: Practical parallel decoding for backscatter communication," *IEEE/ACM Trans. Networking*, vol. 27, no. 1, pp. 330–343, Feb. 2019.

[15] M. Jin, Y. He, X. Meng, D. Fang, and X. Chen, "Parallel Backscatter in the wild: When burstiness and randomness play with you," *IEEE/ACM Trans. Networking*, vol. 29, no. 1, pp. 65–77, Feb. 2021.

[16] S. Chen, S. Zhong, S. Yang, and X. Wang, "A multiantenna RFID reader with blind adaptive beamforming," *IEEE Internet of Things Journal*, vol. 3, no. 6, pp. 986–996, Dec. 2016.

[17] A. Goldsmith, *Wireless Communications*. New York, NY, USA: Cambridge University Press, 2005.

[18] J. Kimionis, A. Bletsas, and J. N. Sahalos, "Increased range bistatic scatter radio," *IEEE Trans. Commun.*, vol. 62, no. 3, pp. 1091–1104, Mar. 2014.

[19] A. Bletsas, A. G. Dimitriou, and J. N. Sahalos, "Improving backscatter radio tag efficiency," *IEEE Trans. Microwave Theory Tech.*, vol. 58, no. 6, pp. 1502–1509, Jun. 2010.

[20] A. Bletsas, J. Kimionis, A. G. Dimitriou, and G. N. Karystinos, "Single-antenna coherent detection of collided FM0 RFID signals," *IEEE Trans. Commun.*, vol. 60, no. 3, pp. 756–766, Mar. 2012.

[21] M. Simon and D. Divsalar, "Some interesting observations for certain line codes with application to RFID," *IEEE Trans. Commun.*, vol. 54, no. 4, pp. 583–586, Apr. 2006.

[22] S. Gollakota and D. Katabi, "Zigzag decoding: Combating hidden terminals in wireless networks," *SIGCOMM Comput. Commun. Rev.*, vol. 38, no. 4, pp. 159–170, Aug. 2008.

[23] J. G. Proakis and M. Salehi, *Digital Communications*, 5th ed. New York, NY: McGraw-Hill, 2007.

[24] M. Nakagami, "The m-distribution - A general formula of intensity distribution of rapid fading," in *Statistical Methods in Radio Wave Propagation*. Pergamon, 1960, pp. 3 – 36.

Konstantinos Skyvalakis received the 5-year Diploma degree in Electrical and Computer Engineering from the Technical University of Crete, Greece, in 2018, where he is currently pursuing his MSc degree. His research interests include methods for low power wireless communications, signal processing for backscatter communication, satellite communications.

Aggelos Bletsas received the Diploma degree (with honors) in Electrical and Computer Engineering from Aristotle University of Thessaloniki, Greece in 1998, and the M.Sc. and Ph.D. degrees from MIT, Cambridge, MA, USA, in 2001 and 2005, respectively. He has worked at Mitsubishi Electric Research Laboratories (MERL), Cambridge, MA and RadioCommunications Laboratory (RCL), Department of Physics, Aristotle University of Thessaloniki. He currently serves as full Professor, School of Electrical & Computer Engineering, Technical University of Crete, Greece. His research interests span the broad area of scalable wireless communications and sensor networking, with emphasis on ultra-low power/cost environmental sensing, backscatter radio and ambiently-powered inference networks. His current focus and contributions are relevant to wireless, batteryless, backscatter sensors for precision agriculture that cost a few Euros, consume a few microWatts and can be read with commodity receivers and smartphones. He has served as Associate Editor of *IEEE Transactions on Wireless Communications* (2015-2021) and *IEEE Wireless Communications Letters* (from foundation in 2011-2016) and Technical Program Committee (TPC) member of major IEEE conferences. Dr. Bletsas was co-recipient of the *IEEE Communications Society 2008 Marconi Prize Paper Award in Wireless Communications*, and various Best Student Paper Awards e.g., in IEEE RFID-TA 2011, IEEE ICASSP 2015, IEEE RFID-TA 2017, MOCAST 2018. He has been included in the Highly-Cited Greek Scientists list. One of his papers is ranked 1st in Google Scholar *Classic Papers in Computer Networks & Wireless Communication*.